Monthly Notices
of the
ROYAL ASTRONOMICAL SOCIETY

MNRAS **490,** 2284–2299 (2019)
Advance Access publication 2019 September 30

doi:10.1093/mnras/stz2725

Testing emission models on the extreme blazar 2WHSP J073326.7+515354 detected at very high energies with the MAGIC telescopes

MAGIC Collaboration: V. A. Acciari,[1,2] S. Ansoldi,[3,4,5,6,7]† L. A. Antonelli,[8] A. Arbet Engels,[9] D. Baack,[10] A. Babić,[11,12,13,14,15]‡ B. Banerjee,[16] U. Barres de Almeida,[17] J. A. Barrio,[18] J. Becerra González,[1,2]★ W. Bednarek,[19] L. Bellizzi,[20] E. Bernardini,[21,22] A. Berti,[23] J. Besenrieder,[24] W. Bhattacharyya,[21] C. Bigongiari,[8] A. Biland,[9] O. Blanch,[25] G. Bonnoli,[20] Ž. Bošnjak,[11,12,13,14,15]‡ G. Busetto,[22] R. Carosi,[26] G. Ceribella,[24] M. Cerruti,[27]★ Y. Chai,[24] A. Chilingaryan,[28] S. Cikota,[11,12,13,14,15]‡ S. M. Colak,[25] U. Colin,[24] E. Colombo,[1,2] J. L. Contreras,[18] J. Cortina,[29] S. Covino,[8] V. D'Elia,[8] P. Da Vela,[26] F. Dazzi,[8] A. De Angelis,[22] B. De Lotto,[3] M. Delfino,[25,30] J. Delgado,[25,30] D. Depaoli,[23] F. Di Pierro,[23] L. Di Venere,[23] E. Do Souto Espiñeira,[25] D. Dominis Prester,[11,12,13,14,15]‡ A. Donini,[3] D. Dorner,[31] M. Doro,[22] D. Elsaesser,[10] V. Fallah Ramazani,[32,33]§ A. Fattorini,[10] G. Ferrara,[8] D. Fidalgo,[18] L. Foffano,[22]★ M. V. Fonseca,[18] L. Font,[34] C. Fruck,[24] S. Fukami,[4,5,6,7]† R. J. García López,[1] M. Garczarczyk,[21] S. Gasparyan,[28] M. Gaug,[34] N. Giglietto,[23] F. Giordano,[23] N. Godinović,[11,12,13,14,15]‡ D. Green,[24] D. Guberman,[25] D. Hadasch,[4,5,6,7]† A. Hahn,[24] J. Herrera,[1,2] J. Hoang,[18] D. Hrupec,[11,12,13,14,15]‡ M. Hütten,[24] T. Inada,[4,5,6,7]† S. Inoue,[4,5,6,7]† K. Ishio,[24] Y. Iwamura,[4,5,6,7]† L. Jouvin,[25] D. Kerszberg,[25] H. Kubo,[4,5,6,7]† J. Kushida,[4,5,6,7]† A. Lamastra,[8] D. Lelas,[11,12,13,14,15]‡ F. Leone,[8] E. Lindfors,[32,33]§ S. Lombardi,[8] F. Longo,[3,35] M. López,[18] R. López-Coto,[22] A. López-Oramas,[1,2] S. Loporchio,[23] B. Machado de Oliveira Fraga,[17] C. Maggio,[34] P. Majumdar,[16] M. Makariev,[36] M. Mallamaci,[22] G. Maneva,[36] M. Manganaro,[11,12,13,14,15]‡ K. Mannheim,[31] L. Maraschi,[8] M. Mariotti,[22] M. Martínez,[25] D. Mazin,[4,5,6,7,24]† S. Mićanović,[11,12,13,14,15]‡ D. Miceli,[3] M. Minev,[36] J. M. Miranda,[20] R. Mirzoyan,[24] E. Molina,[27] A. Moralejo,[25] D. Morcuende,[18] V. Moreno,[34] E. Moretti,[25] P. Munar-Adrover,[34] V. Neustroev,[32,33]§ C. Nigro,[21] K. Nilsson,[32,33]§ D. Ninci,[25] K. Nishijima,[4,5,6,7]† K. Noda,[4,5,6,7]† L. Nogués,[25] S. Nozaki,[4,5,6,7]† S. Paiano,[22] J. Palacio,[25] M. Palatiello,[3] D. Paneque,[24] R. Paoletti,[20] J. M. Paredes,[27] P. Peñil,[18] M. Peresano,[3] M. Persic,[3,37] P. G. Prada Moroni,[26] E. Prandini,[22] I. Puljak,[11,12,13,14,15]‡ W. Rhode,[10] M. Ribó,[27] J. Rico,[25] C. Righi,[8] A. Rugliancich,[26] L. Saha,[18] N. Sahakyan,[28] T. Saito,[4,5,6,7]† S. Sakurai,[4,5,6,7]† K. Satalecka,[21] K. Schmidt,[10] T. Schweizer,[24] J. Sitarek,[19] I. Šnidarić,[11,12,13,14,15]‡ D. Sobczynska,[19] A. Somero,[1,2] A. Stamerra,[8] D. Strom,[24] M. Strzys,[24] Y. Suda,[24]

★ E-mail: luca.foffano@phd.unipd.it (LF); matteo.cerruti@icc.ub.edu (MC); jbecerragonzalez@gmail.com (JBG)
† Japanese MAGIC Consortium
‡ Croatian Consortium
§ Finnish MAGIC Consortium

© 2019 The Author(s)
Published by Oxford University Press on behalf of the Royal Astronomical Society

Downloaded from https://academic.oup.com/mnras/article/490/2/2284/5579033 by guest on 10 June 2024

T. Surić,[11,12,13,14,15]‡ M. Takahashi,[4,5,6,7]† F. Tavecchio,[8] P. Temnikov,[36] T. Terzić,[11,12,13,14,15]‡ M. Teshima,[4,5,6,7,24]† N. Torres-Albà,[27] L. Tosti,[23] V. Vagelli,[23] J. van Scherpenberg,[24] G. Vanzo,[1,2] M. Vazquez Acosta,[1,2] C. F. Vigorito,[23] V. Vitale,[23] I. Vovk,[24] M. Will,[24] D. Zarić,[11,12,13,14,15]‡ External Collaborators: K. Asano,[4,5,6,7]† and F. D'Ammando[38] R. Clavero[1,2]

Affiliations are listed at the end of the paper

Accepted 2019 September 25. Received 2019 September 24; in original form 2019 August 9

ABSTRACT

Extreme high-energy-peaked BL Lac objects (EHBLs) are an emerging class of blazars. Their typical two-hump-structured spectral energy distribution (SED) peaks at higher energies with respect to conventional blazars. Multiwavelength (MWL) observations constrain their synchrotron peak in the medium to hard X-ray band. Their gamma-ray SED peaks above the GeV band, and in some objects it extends up to several TeV. Up to now, only a few EHBLs have been detected in the TeV gamma-ray range. In this paper, we report the detection of the EHBL 2WHSP J073326.7+515354, observed and detected during 2018 in TeV gamma rays with the MAGIC telescopes. The broad-band SED is studied within an MWL context, including an analysis of the *Fermi*-LAT data over 10 yr of observation and with simultaneous *Swift*-XRT, *Swift*-UVOT, and KVA data. Our analysis results in a set of spectral parameters that confirms the classification of the source as an EHBL. In order to investigate the physical nature of this extreme emission, different theoretical frameworks were tested to model the broad-band SED. The hard TeV spectrum of 2WHSP J073326.7+515354 sets the SED far from the energy equipartition regime in the standard one-zone leptonic scenario of blazar emission. Conversely, more complex models of the jet, represented by either a two-zone spine-layer model or a hadronic emission model, better represent the broad-band SED.

Key words: galaxies: active – BL Lacertae objects: general – gamma-rays: galaxies – X-rays: general.

1 INTRODUCTION

Blazars are active galactic nuclei (AGNs) with relativistic jets closely aligned with the line of sight of the observer. Their spectral energy distributions (SEDs) generally consist of two main non-thermal components. Typically, the first component is ascribed to synchrotron radiation emitted by relativistic electrons moving within the jet. Different scenarios have been proposed to explain the nature of the second hump peaking at higher energies. The standard leptonic scenario suggests that this second hump is produced by inverse Compton (IC) scattering of low-energy photons (Rees 1967). In the Synchrotron-Self-Compton (SSC) model (e.g. Maraschi, Ghisellini & Celotti 1992; Tavecchio, Maraschi & Ghisellini 1998), this photon field may be composed by the synchrotron emission responsible for the first SED hump. Additionally, this high-energy hump might be associated with external photon fields that are up-scattered by IC scattering in the External Compton scenario (Dermer & Schlickeiser 1993).

Relativistic protons might also be accelerated in the blazar jet. When sufficiently high energies are reached to allow photopion production, electromagnetic cascades will develop and contribute to the emission of the high-energy hump, in addition to proton, muon, and pion synchrotron radiation (Mannheim 1993; Boettcher 2010). Moreover, in the so-called hadronic cascade scenario, ultra-high energy cosmic rays (UHECRs) might interact in the intergalactic space through photohadronic reactions and produce photons that contribute to the high-energy hump (e.g. Essey & Kusenko 2010; Murase et al. 2012; Tavecchio 2014). Finally, this second hump may be also produced by a combination of leptonic and hadronic processes.

Blazars are historically subdivided into two main categories. The objects that show broad emission lines in their optical spectrum are classified as flat spectrum radio quasars (FSRQs). When these lines have an equivalent width of less than 5 Å, blazars are defined as BL Lac objects. It has been suggested that blazars follow the so-called 'blazar sequence' (Fossati et al. 1998), based on the anticorrelation between the bolometric luminosity and the peak energy of their SED humps (Ghisellini 1999; Ghisellini & Tavecchio 2008; Ghisellini et al. 2017). Conversely, some authors argue that the blazar sequence might be due to selection effects (see e.g. Antón & Browne 2005; Giommi et al. 2012). The FSRQs, whose synchrotron peak is located at low frequencies, are the 'redder' blazars. The BL Lac objects populate the sequence at higher frequencies. Blazars are further divided in sub-classes depending on the frequency of the synchrotron peak $\nu_{\rm peak}^{\rm sync}$: they are classified as low-peaked objects (LBL, with $\nu_{\rm peak}^{\rm sync} < 10^{14}$ Hz), intermediate-peaked objects (IBL, with $\nu_{\rm peak}^{\rm sync}$ between 10^{14} and 10^{15} Hz), and high-peaked objects

Downloaded from https://academic.oup.com/mnras/article/490/2/2284/5579033 by guest on 10 June 2024

(HBL, $\nu^{\rm sync}_{\rm peak}$ between 10^{15} and 10^{17} Hz), according to Abdo et al. (2010).

Costamante et al. () proposed a new class of BL Lac objects with extreme spectral properties and located at the very edge of the blazar sequence, named extreme high-frequency-peaked blazars (EHBLs). In this work, we will use the definition of EHBL based on the synchrotron peak position $\nu^{\rm sync}_{\rm peak}$ located above 10^{17} Hz.

The archetypal EHBL is 1ES 0229+200.

Its archival SED has been observed in detail by several multi-wavelength (MWL) observational campaigns during the last years, and shows the key features of this class of objects. In fact, in the EHBLs the synchrotron hump is shifted towards high energies with respect to conventional blazars, making the thermal optical radiation of the host galaxy visible for low-redshift objects.

The synchrotron peak located in the medium-to-hard X-ray band pushes the second SED peak to the very-high-energy gamma-ray band (VHE, energies above 100 GeV). For this reason, EHBLs are generally supposed to be faint in high-energy (HE, energies between 100 MeV and 100 GeV) gamma rays (Tavecchio et al. 2010). The intrinsic spectrum of 1ES 0229+200 at VHE is the hardest ever measured (e.g. Aharonian et al. 2007c; Aliu et al. 2014). Similar hard spectra have been reported for few other sources, like for example 1ES 0347−121 (Aharonian et al. 2007b), RGB J0710+591 (Acciari et al. 2010), and 1ES 1101−232 (Aharonian et al. 2007a). In these objects, the peak of the second hump extends beyond several TeV, and for this reason they have also been called 'hard-TeV blazars' by Costamante et al. (2018).

This feature makes their SEDs challenging for the standard one-zone leptonic SSC model. In that scenario, the model would suggest rather soft SSC spectra at TeV energies due to the decreasing scattering cross-section with energy in the Klein–Nishina regime (Tavecchio et al. 2009). In order to explain such a shift in the SED peaks, the minimum Lorentz factor of the electron energy distribution $\gamma_{\rm min}$ has to be very high and the magnetic field intensity B is required to be very low with respect to the standard values inferred in classical TeV BL Lac objects (Tavecchio et al. 2010; Lefa, Rieger & Aharonian 2011).

To explain the hard-TeV spectra in EHBLs, different alternative models have been proposed. Saugé & Henri (2004) and Lefa et al. (2011), for example, adopt extremely hard Maxwellian particle distributions, while Katarzynski et al. (2006) and Tavecchio et al. (2009) use a low-energy cut-off of the electron distribution at VHE. In the case of 1ES 0229+200, the intergalactic cascades scenario (Murase et al. 2012) was successfully applied to explain the hard TeV spectrum. Finally, due to the evidence of scarce and low-amplitude flux variability and their hard TeV gamma-ray spectra, EHBLs turn out to be interesting candidates for hadronic and lepto-hadronic emission models that can well reproduce their observed SEDs (e.g. Murase et al. 2012; Cerruti et al. 2015).

The hard VHE gamma-ray spectrum of EHBLs extending up to several TeV – as that observed in sources like 1ES 0229+200 – is also an important probe for testing models of the extragalactic background light (EBL, see e.g. Hauser & Dwek 2001) and of the intergalactic magnetic fields (IGMF, e.g. Vovk et al. 2012).

MWL observations have revealed that other EHBL objects have high synchrotron peak frequencies similar to 1ES 0229+200, but much softer TeV spectra with an IC hump clearly peaking in the GeV to TeV band (e.g. Costamante et al. 2001b, 2018). Additionally, some very bright HBL sources (like, for example, Mrk 501) have shown EHBL-like behaviour during some flaring episodes (Pian et al. 1998; Ahnen et al. 2018). Hence, the EHBL class might be a complex population of sources, characterized by different spectral properties (Foffano et al. 2019), or even associated to high-activity states of some blazars.

Hard-TeV blazars are the EHBL sources with the highest IC peak frequency, and the difficulties in modelling their SEDs are generally related to this extreme spectral property. However, EHBLs with a more moderate IC peak located below a few TeV might be good candidates for testing theoretical models. The successful application of theoretical models to different EHBLs might help in understanding why the high synchrotron peak is not always correlated with a hard VHE spectrum, and might help to unveil the origin of the extreme particle acceleration mechanism of this class. The differences in the spectral properties we find in the EHBL category and the low number of known objects of this class motivate their monitoring and the search for new candidates.

An accurate description of the broad-band spectrum is essential to understand the origin of the extreme SED properties of EHBLs, especially in the gamma-ray band. For example, dedicated studies have been recently carried out in the HE gamma-ray band performing detailed analyses of faint *Fermi*-LAT sources (Arsioli et al. 2018). In this framework, the TeV gamma-ray band plays a key role in the EHBLs characterization. However, up to now only a few such sources have been observed and characterized in the VHE gamma-ray regime. New TeV observations of EHBL objects are needed in order to increase the EHBL population and possibly disclose the physical interpretation of such extreme spectral properties.

In this paper, we provide a set of new VHE gamma-ray observations on an EHBL named 2WHSP J073326.7+515354. This blazar, also named PGC 2402248, has been selected from the 2WHSP catalogue (Chang et al. 2017) on the basis of its high synchrotron peak frequency equal to $\nu^{\rm sync}_{\rm peak,2WHSP} = 10^{17.9}$ Hz. It is associated with the *Fermi*-LAT source 3FGL J0733.5+5153 in the 3FGL catalogue (Acero et al. 2015) as active galaxy of uncertain type, and reported in the 3FHL catalogue (Ajello et al. 2017) as associated with the source 3FHL J0733.4+51523 with a spectral index of $\Gamma_{\rm HE} = 1.34 \pm 0.43$. Additionally, the source 2WHSP J073326.7+515354 is compatible with the position (at 2.4 arcmin) of the source SWIFT J0733.9+5156 (position uncertainty 5.67 arcmin), which is reported also in the *Swift*-BAT 105-month catalogue (Oh et al. 2018). In this catalogue, the reported flux of the source is $8.17^{10.44}_{6.00} \times 10^{-12}$ erg cm^{-2} s^{-1} with a spectral index of $2.32^{3.25}_{1.61}$.

The MAGIC observations led to the first detection of this source in TeV gamma rays on 2018 April 19 (Mirzoyan 2018). During the MAGIC pointings, simultaneous observations were performed by the KVA, *Swift*-UVOT/XRT, and *Fermi*-LAT telescopes. Additionally, optical data were collected with the Gran Telescopio Canarias (GTC) in order to estimate the redshift of the source that was previously unknown. The new measurement of the redshift of 2WHSP J073326.7+515354 was reported as $z = 0.065$ (Becerra Gonzalez et al. 2018). This value is particularly important for the estimation of the intrinsic gamma-ray spectrum of the source, and consequently for testing the theoretical emission models of the broad-band SED.

The structure of this paper is as follows: in Section 2, we describe the observations and results from the MAGIC observations. In addition, simultaneous observations performed by KVA, *Swift*, and the long-integration analysis of the *Fermi*-LAT telescope data are presented. In Section 3 the variability at different frequencies is discussed. In Section 4, we report the collected broad-band SED and a discussion about the observational properties of the source.

Downloaded from https://academic.oup.com/mnras/article/490/2/2284/5579033 by guest on 10 June 2024

In Section 5, we provide a discussion on the modelling of the SED, performed by means of leptonic and hadronic models. Finally, we report in Section 6 the conclusions of this work and future prospects. We adopt $H_0 = 67\,\mathrm{km\,s^{-1}\,Mpc^{-1}}$, $\Omega_\Lambda = 0.7$, $\Omega_M = 0.3$ (Planck Collaboration VI 2018).

2 OBSERVATIONS AND RESULTS

2WHSP J073326.7+515354 was observed in the VHE gamma-ray band with the MAGIC telescopes, in the optical and UV bands with the KVA telescope and *Swift*-UVOT and in the X-ray band with *Swift*-XRT. Additionally, an analysis of the sample collected by *Fermi*-LAT during more than 10 yr of operation was performed.

2.1 The MAGIC telescopes

MAGIC (Aleksić et al. 2016a) is a system of two Imaging Air-shower Cherenkov Telescopes (IACTs) designed to indirectly detect gamma rays through the Cherenkov emission of the charged component of the extensive air shower they generate interacting with Earth's atmosphere. The two telescopes are located on the Canary island of La Palma, at 2200 m altitude. Their large reflective surface of 17 m diameter each allows the MAGIC telescopes to reach, under good observational conditions, an energy threshold as low as 50 GeV when operated in standard trigger mode. The integral sensitivity for point-like sources above 220 GeV, assuming a Crab Nebula-like spectrum, is (0.66 ± 0.03) per cent of the Crab Nebula flux in 50 h of observations. At those energies the angular resolution is 0.07 deg, while the energy resolution reaches 16 per cent. The performance of the instrument and the details on the data analysis procedure are fully described in Aleksić et al. (2016b) and references therein.

2.1.1 Observations

MAGIC observed the source 2WHSP J073326.7+515354 for a total of 23.4 h in 2018 within an observational program aimed at searching for new EHBLs in the TeV gamma-ray band. The observations were performed during 25 nights from 2018 January 23 to 2018 April 19 (MJD 58141-58227), with zenith angle range between 23° and 40° and good data quality. The data have been analysed using the MAGIC Analysis and Reconstruction Software (MARS, Moralejo et al. 2009; Aleksić et al. 2016b).

2.1.2 Signal search

The emission from a source in VHE gamma rays can be evaluated by means of the so-called θ^2 plot. The θ^2 parameter is defined as the squared angular distance between the reconstructed incoming direction of the gamma-ray event and the nominal position of the source in camera coordinates. The typical signature of VHE point-like sources, after the application of energy-dependent background suppression cuts, is an excess at low θ^2 values. In general, a source is considered detected in the VHE gamma-ray range, if the significance of the excess of gamma-like events over background events exceeds $5\,\sigma$. The significance of the gamma-ray signal is estimated with formula no. 17 of Li & Ma (1983).

The θ^2 plot for 2WHSP J073326.7+515354 is shown in Fig. 1(a). An excess of 95 ± 16 events in the standard fiducial signal region with $\theta^2 < 0.009$ deg^2 is found, corresponding to a significance of $6.76\,\sigma$. The θ^2 distribution shows a fluctuation of the gamma-like events with respect to the background events in the region from 0.04 to 0.12 deg^2. In order to investigate whether this fluctuation is significant, we compare the θ^2 distribution for 2WHSP J073326.7+515354 with regards to the reference point spread function (PSF) obtained from a Crab Nebula data sample observed contemporaneously to 2WHSP J073326.7+515354. The PSF was also rescaled to the 2WHSP J073326.7+515354 spectrum and zenith distribution. Following Da Vela et al. (2018), the PSF and the θ^2-plot of 2WHSP J073326.7+515354 were fitted with the King function, and a comparison among the parameters was performed. The fit has been performed up to $\theta^2 = 0.45$ deg^2. The PSF computed for 2WHSP J073326.7+515354 is consistent (χ^2/DOF = 89/98) with the reference PSF of the instrument. In Fig. 1(b) the residuals plot of the fit is shown. This check confirms that the possible mismatch with the background in the region from 0.04 to 0.12 deg^2 is not statistically significant, and represent a casual fluctuation of the background.

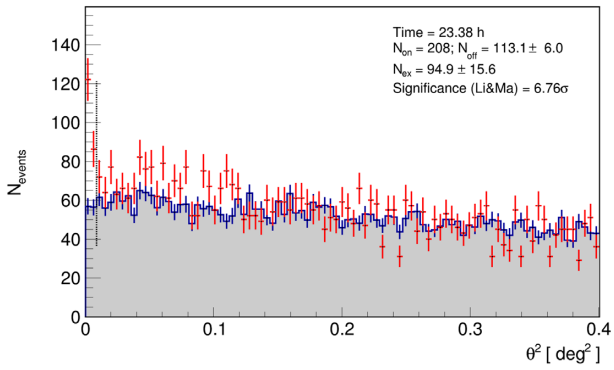

(a) θ^2 plot.

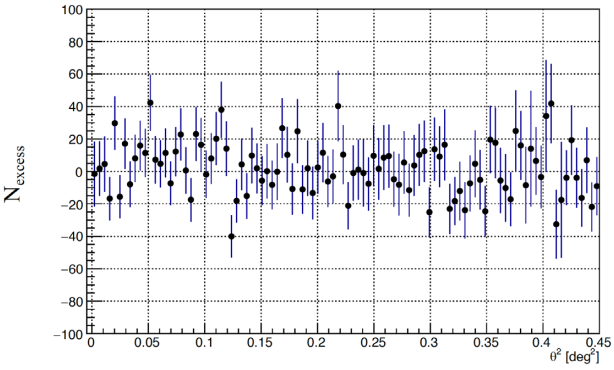

(b) Residuals plot.

Figure 1. (a) The θ^2 distribution from the direction of 2WHSP J073326.7+515354 as observed by the MAGIC telescopes is shown. The gamma-ray like events are represented by the red markers, while the background is denoted by the shadowed grey area. The vertical dashed line indicates the defined signal region to which the significance of the detection is calculated. (b) The residuals of the observed data with respect to the fit with the reference PSF of the instrument is shown.

2.1.3 Spectrum

The spectrum of the source 2WHSP J073326.7+515354 observed with the MAGIC telescopes, reported in Fig. 2, was reconstructed between 0.1 and 8 TeV using the Tikhonov unfolding method

Downloaded from https://academic.oup.com/mnras/article/490/2/2284/5579033 by guest on 10 June 2024

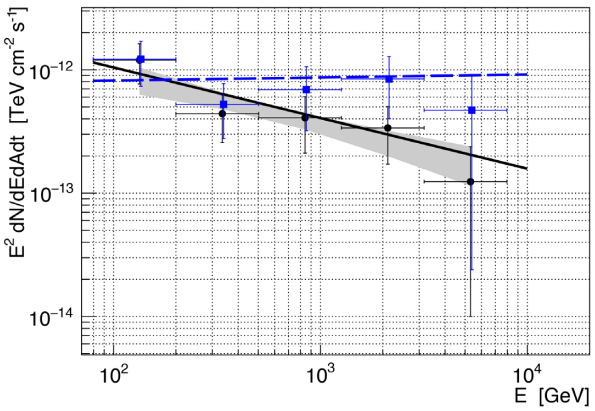

Figure 2. VHE SED from 2WHSP J073326.7+515354. The black markers and line represent the observed SED spectral points and fit. The intrinsic SED after correcting for the EBL absorption assuming the model from Dominguez et al. (2011) is represented in blue. The shaded area represents the uncertainty obtained from a forward folding method (Mizobuchi et al. 2005).

(Albert et al. 2007) in order to include migrations between true and reconstructed energy. It can be described by a simple power-law model ($\chi^2/\mathrm{DOF} = 2.4/3$):

$$\frac{\mathrm{dN}}{\mathrm{dE}} = \mathrm{f_0}\left(\frac{\mathrm{E}}{200\ \mathrm{GeV}}\right)^{-\Gamma},$$

where the observed photon index is $\Gamma_{\mathrm{obs}} = 2.41 \pm 0.17_{\mathrm{stat}}$, and the corresponding normalization constant $\mathrm{f_{0,obs}} = (1.95 \pm 0.10_{\mathrm{stat}}) \times 10^{-11}$ ph cm^{-2} s^{-1} TeV^{-1} at the energy of 200 GeV. A detailed discussion on the systematic uncertainties can be found in Aleksić et al. (2016b).

The intrinsic spectrum, after correcting for the absorption due to the interaction with the EBL according to the model by Dominguez et al. (2011), can be fitted with a power-law function ($\chi^2/\mathrm{DOF} = 2.8/3$) with a photon index $\Gamma_{\mathrm{intr}} = 1.99 \pm 0.16$ and a normalization constant $\mathrm{f_{0,intr}} = (2.03 \pm 0.13) \times 10^{-11}$ ph cm^{-2} s^{-1} TeV^{-1} at the same energy of 200 GeV. Other EBL models applied to correct the data provide compatible results.

Since the resulting SED from 2WHSP J073326.7+515354 at VHE is substantially flat, the source has a second hump likely peaking at few TeV (see later for further details). This is a first difference with respect to the hard-TeV blazars of Costamante et al. (2018), which show continuously increasing flux up to at least several TeV and hard spectral index of the order of 1.5 ∼ 1.7. A summary of the source characteristics and results from the VHE data analysis can be found in Table 1. The flux results above 200 GeV as a function of the observation time are given in Table A1.

2.2 *Fermi*-LAT data analysis

The pair-conversion Large Area Telescope (LAT) onboard the *Fermi* satellite monitors the gamma-ray sky in survey mode every three hours in the energy range from 20 MeV to > 300 GeV (Atwood et al. 2009). For this work, a region of interest (ROI) centred around 2WHSP J073326.7+515354 (4FGL J0733.4+5152) with a radius of 7 arcsec was selected. The data sample included more than 10 yr of data collected by *Fermi*-LAT, from 2008 August 4 to 2019 June 24 (MJD 54682-58658). The data reduction of the events of the Pass8 `source` class was performed with the Science-Tools software package version v11r5p3 in the energy range 0.5–300 GeV. To reduce Earth limb contamination a zenith angle cut of 90° was applied to the data. The binned likelihood fit of the data was performed using the recommended Galactic diffuse emission model (see e.g. Acero et al. 2016) and isotropic component recommended for Pass8 (P8R2) `source` event class.[1]

The normalizations of both diffuse components in the source model were allowed to freely vary during the spectral fitting. In addition to the source of interest, all the sources included in the 4FGL catalogue (The Fermi-LAT collaboration 2019) within a distance of 14 deg from the source of interest were included. We build the likelihood model including all the 4FGL sources within 14 deg from the position. For the likelihood minimization we leave free to vary the spectral parameters of the sources in the region within five degrees from the centre of the ROI and fixed them to their catalogue values outside. The binned likelihood fit was carried out in two steps, After a first fit, the targets with test statistics (TS) < 2 were removed from the model. After that cut, a final likelihood fit was carried out. We did not find significant residuals, which could suggest the presence of additional sources in the ROI. 2WHSP J073326.7+515354 was detected with a TS = 138.8, a flux of $F(0.5\text{–}300\ \mathrm{GeV}) = (1.3 \pm 0.5) \times 10^{-9}$ ph cm^{-2} s^{-1} and a hard spectral index of $\Gamma = 1.73 \pm 0.11$ (compatible with the value reported in the 4FGL catalogue, $\Gamma_{\mathrm{4FGL}} = 1.80 \pm 0.10$). The same analysis is carried out in two-year time bins to study the flux evolution of the source. The results are shown in Table A2.

2.3 *Swift* data analysis

During the MAGIC observation campaign, simultaneous optical-UV and X-ray observations were performed with the *Neil Gehrels Swift Observatory (Swift)* via a Target of Opportunity (ToO) request.

2.3.1 *XRT instrument*

The X-ray Telescope (*XRT*, Burrows et al. 2004) onboard *Swift* acquired eight good quality raw data sets.[2] These eight observations cover the period between 2018 January 26 (MJD 58144.08) and 2018 April 29 (MJD 58227.92), and have a total exposure time of ∼ 2.7 h with an average of 1.2 ks per observation. The observation data were analysed based on the standard *Swift* analysis procedure described by Evans et al. (2009) using the configuration described by Fallah Ramazani, Lindfors & Nilsson (2017) for the photon counting observation mode and assuming a fixed equivalent Galactic hydrogen column density of $N_{\mathrm{H}} = 5.12 \times 10^{20}$ cm^{-2} (Kalberla et al. 2005).

The spectra for each individual daily observation were fitted by a power-law and a log-parabola function. In all cases, the log-parabola fit did not improve significantly the result (lower than 3σ confidence level, C.L.) with respect to the power-law fit. The results of this analysis are reported in Table A3 together with data obtained by *Swift*-XRT since 2009. The X-ray spectrum of the source is hard, with a photon index $1.5 \leq \Gamma_X \leq 1.6$ on the data strictly simultaneous to the MAGIC campaign, but with hint of a softer spectrum in the archival data with larger uncertainty.

[1] https://fermi.gsfc.nasa.gov/ssc/data/access/lat/BackgroundModels.html
[2] https://swift.gsfc.nasa.gov/analysis/threads/gen_thread_attfilter.html

Downloaded from https://academic.oup.com/mnras/article/490/2/2284/5579033 by guest on 10 June 2024

Table 1. Summary of the observational results obtained with the MAGIC telescopes. We report here the source name, its coordinates, and the first estimation of redshift reported by Becerra Gonzalez et al. (2018). The information related to MAGIC observations includes the observation time, the resulting significance of the detection, and the integral flux above 200 GeV. Finally, the observed spectral index Γ_{obs} as measured by MAGIC is reported together with the intrinsic one Γ_{intr}, deabsorbed with the EBL model by Dominguez et al. (2011).

Source name	R.A. deg	δ deg	Redshift	Obs. time	Significance	Integral flux > 200 GeV 10^{-13} ph cm^{-2} s^{-1}	Γ_{obs}	Γ_{intr}
2WHSP J073326.7+515354	113.36125	51.89889	0.065	23.38 h	6.76 σ	22.5 ± 0.60	2.41 ± 0.17	1.99 ± 0.16

2.3.2 *UVOT observations*

During the *Swift* pointings in 2018, the UVOT instrument observed 2WHSP J073326.7+515354 in its optical (*U*) and UV (*W1* and *W2*) photometric bands (Poole et al. 2008; Breeveld et al. 2010). We analysed the data using the `uvotsource` task included in the HEASOFT package (v6.23). Source counts were extracted from a circular region of 5 arcsec radius centred on the source, while background counts were derived from a circular region of 20 arcsec radius in a nearby source-free region. The observed magnitudes are corrected for extinction using the $E(B-V)$ value of 0.50 from Schlafly & Finkbeiner (2011) and the extinction laws from Cardelli, Clayton & Mathis (1989) and converted to flux densities. The results for each individual observation are shown in Table A4.

2.4 KVA data analysis

The Tuorla blazar monitoring program[3] has observed 2WHSP J073326.7+515354 coordinated with the MAGIC observations since 2018 April. These observations were performed in the *R* band (Cousins) by the 35 cm telescope attached to the Kungliga Vetenskapsakademien Academy (KVA) system. The data were analysed using the differential photometry method described by Nilsson et al. (2018). In order to perform differential photometry, the comparison stars were selected in the same field of view (reported in Fig. 3). To measure their magnitude, the source was observed among many other blazars with known comparison stars on the night of 2018 April 2. The results of the calibration in the *R* band of the comparison stars in Fig. 3 are: star no. 1 with magnitude 13.11, star no. 2 with magnitude 14.29, star no. 3 with magnitude 11.93, and star no. 4 with magnitude 13.63. The average zero-point of the night was calculated from the photometric zero-point magnitude of each image using constant aperture taking into account the effect of airmass.

The contribution of the host galaxy flux is calculated by combining 55 good quality images taken by the KVA telescope. The images are treated for bias, dark, flat-fielding, and fringe map corrections. A Markov Chain Monte Carlo ensemble sampler (e.g Martino & Elvira 2017) was used to map an *a posteriori* distribution in the three-dimensional parameter space. The resulting images are aligned using the stars in the FoV and the median combining method. The combined image has a total exposure of 5500 s with a full width at half-maximum of FWHM= 3.0 arcsec. The comparison star no. 3 (Fig. 3) was used to calibrate the field. Following the method described in MAGIC Collaboration (2018), we use the combined deep *R*-band image to search for the host galaxy emission.

In order to study its host galaxy, we fitted two-dimensional surface brightness models to the light distribution of 2WHSP J073326.7+515354. First, we fit a point source model (with three free parameters, i.e. the source x–y positions and the nucleus flux) with the Sersić index equal to 4 to fix the position of the nucleus. A second fit was performed with a model of a point source and an elliptical host galaxy of ellipticity equal to zero. The positions determined in the first model were used as first-order approximation for the position of the core and the host galaxy. Both models were convolved with the PSF which was determined from the comparison with star no. 3. The fits were made to pixels within 18 pix from the centre of 2WHSP J073326.7+515354. We employed 50 independent walkers, each completing 2000 iteration steps and with flat priors. The best-fitting (mode of the posteriors) parameters of the second model are host galaxy flux $R_{host} = 14.88$ mag and effective radius $r_{eff} = 6.8$ arcsec. The core flux in the *R*-band optical is $R_{core} = 17.36$ mag. From these data, the host galaxy flux within an aperture of 5 arcsec is $F_{host} = 1.38$ mJy.

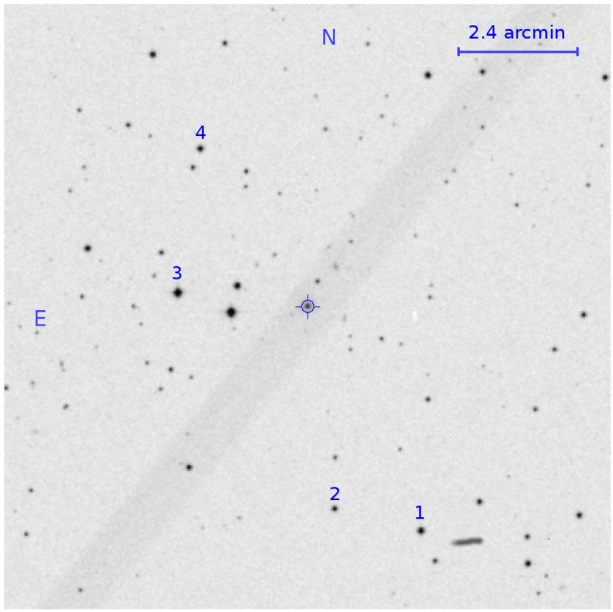

Figure 3. Finding chart of 2WHSP J073326.7+515354 for the optical photometry and host galaxy measurement. It has been produced from the Digitized Sky Survey (DSS) images using SkyView (The Internet's Virtual Telescope, https://skyview.gsfc.nasa.gov/current/cgi/titlepage.pl).

The results of the Tuorla blazar monitoring are presented in Table A5. They are corrected for Galactic extinction using values from Schlafly & Finkbeiner (2011) and the host galaxy contribution.

3 VARIABILITY

The MWL light curve from optical to VHE gamma rays is shown in Fig. 4. The X-ray observations allow us to study the variability of the synchrotron flux and the peak of its emission, while the gamma-ray light curve from MAGIC can be used to infer the flux evolution in the high-energy peak. Since the light curve from *Fermi*-LAT

[3] http://users.utu.fi/kani/1m

Downloaded from https://academic.oup.com/mnras/article/490/2/2284/5579033 by guest on 10 June 2024

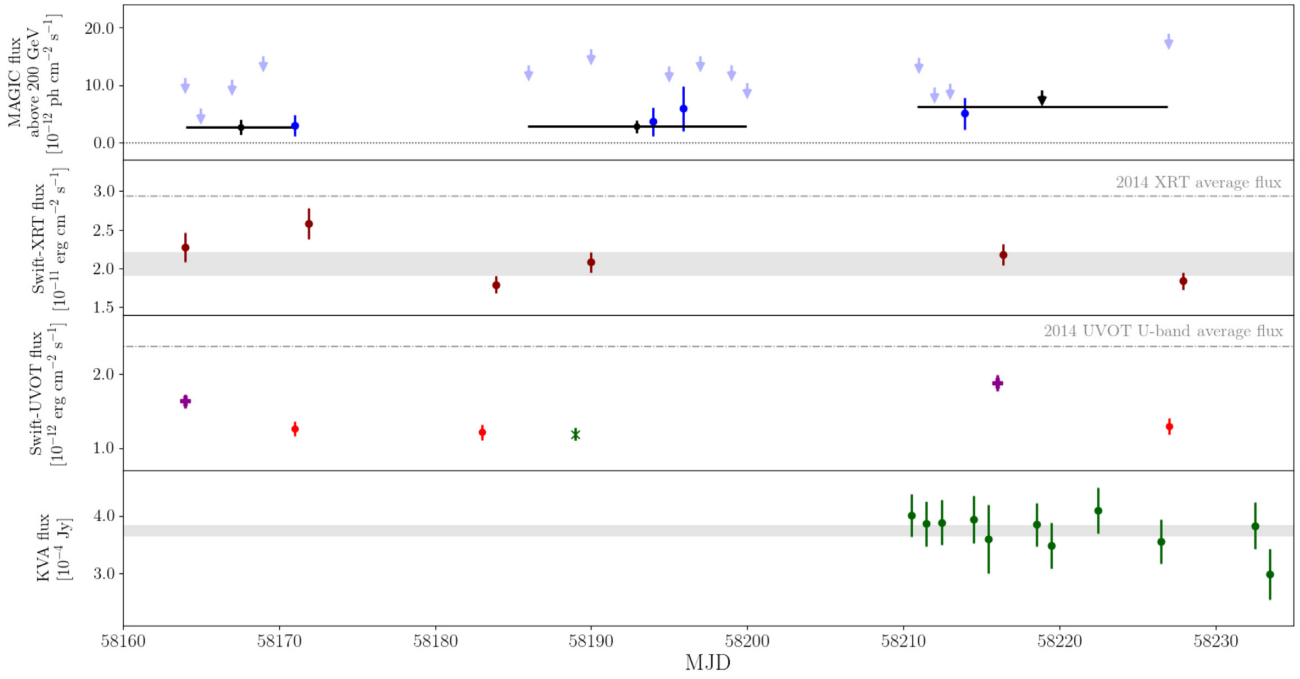

Figure 4. MWL light curve of 2WHSP J073326.7+515354 during the MAGIC observation campaign. In order from top to bottom, we present the MAGIC flux and 95 per cent C.L. upper limits (arrows) above 200 GeV, the *Swift*-XRT 0.3–10 keV flux points, the *Swift*-UVOT points (in the *U* band in violet, *W1* band in red, and *W2* band in dark green), and the KVA optical flux points (after host galaxy subtraction). For the X-ray and optical energy bands, we report in light grey the 1σ band around the average flux. The MAGIC flux has been computed in night-wise (in blue) and monthly binning (black). For the X-ray and UV energy bands, we report in dashed light grey lines the highest average flux obtained during 2014 observations. Due to the low flux emitted by the source in the HE band, the light curve as observed by the *Fermi*-LAT can only be produced in large time bins larger than the scale shown in this figure.

has been computed on large time bins of two years over all 10 yr of observations, we report in Table A2 the flux and photon index measurements in this energy band.

In the optical band, the KVA observations during the MAGIC campaign were carried out in the *R* filter. The results are compatible with a constant flux of 3.74 ± 0.1 mJy, yielding a χ^2/DOF of 6.6/11.

In the UV band, as observed by *Swift*-UVOT with filters *U*, *W1*, and *W2*, even though the statistics are sparse, no strong flux variations were detected over the course of the MAGIC observation campaign. The flux is compatible with a constant fit of $(1.3 \pm 0.2) \times 10^{-12}$ erg cm^{-2} s^{-1} with χ^2/DOF of 0.5/3 and $(1.76 \pm 0.05) \times 10^{-12}$ erg cm^{-2} s^{-1} with χ^2/DOF of 4.6/4 for the bands *W1* and *U*, respectively. For the band *W2*, only one observation is available during that period, and therefore no conclusion for variability can be derived. As reported in Table A4, in comparison with historical observations from 2009 and 2011, the source shows fluxes compatible with the average fluxes reported above. However, during January 2014 the source showed fluxes higher by a factor of about four to five times compared to the average flux during the MAGIC observation window in both the *U* and *W2* bands.

The X-ray observations performed by *Swift*-XRT during the MAGIC observation campaign show moderate variability. A constant fit to the flux evolution during that period can be discarded at a 3.7σ C.L. (χ^2/DOF of 29.6/8). The previous observations of the source carried out between 2009 and 2014 show a flux range of 1 to 3×10^{-12} erg cm^{-2} s^{-1}. When considering only simultaneous XRT and MAGIC observations (MJD 58144, 58164, 58190, and 58227), the flux is compatible with a constant average flux of $(2.07 \pm 0.15) \times 10^{-11}$ erg cm^{-2} s^{-1} (χ^2/DOF of 6.8/4). A marginal 'harder-when-brighter' trend is found in the flux versus spectral index observed in the X-ray band by *Swift*, as shown in Fig. 5. The trend can be fitted by a linear function with χ^2/DOF of 1.3/13) with slope of -1.64 ± 0.62. This trend is quite typical in BL Lacs, and has been observed in several X-ray campaigns of Mrk 501 and Mrk 421 (e.g. Pian et al. 1998; Ahnen et al. 2018).

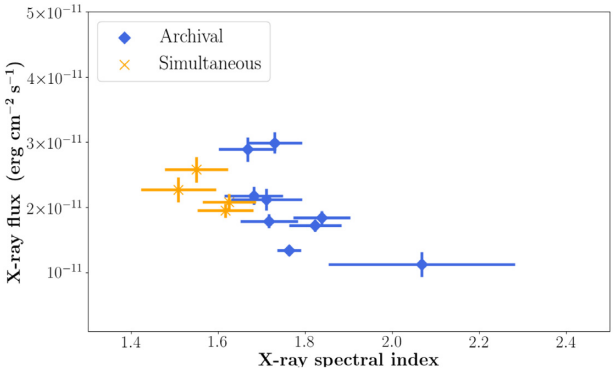

Figure 5. The X-ray 0.3–10 keV integral flux as a function of the spectral index measured with *Swift*-XRT during all the previous non-simultaneous observations of the source (in blue) and the ones simultaneous to MAGIC observations (yellow).

Finally, in the *Swift*-BAT 105-month catalogue (Oh et al. 2018) the source is detected with a signal-to-noise ratio (SNR) of only 5.38, and no variability is reported.

Regarding the high-energy SED peak, the light curve is limited due to the low flux of the target. For the flux evolution of the HE gamma rays observed by *Fermi*-LAT, a time bin of two years was used in order to collect enough photon statistics. As shown in

Downloaded from https://academic.oup.com/mnras/article/490/2/2284/5579033 by guest on 10 June 2024

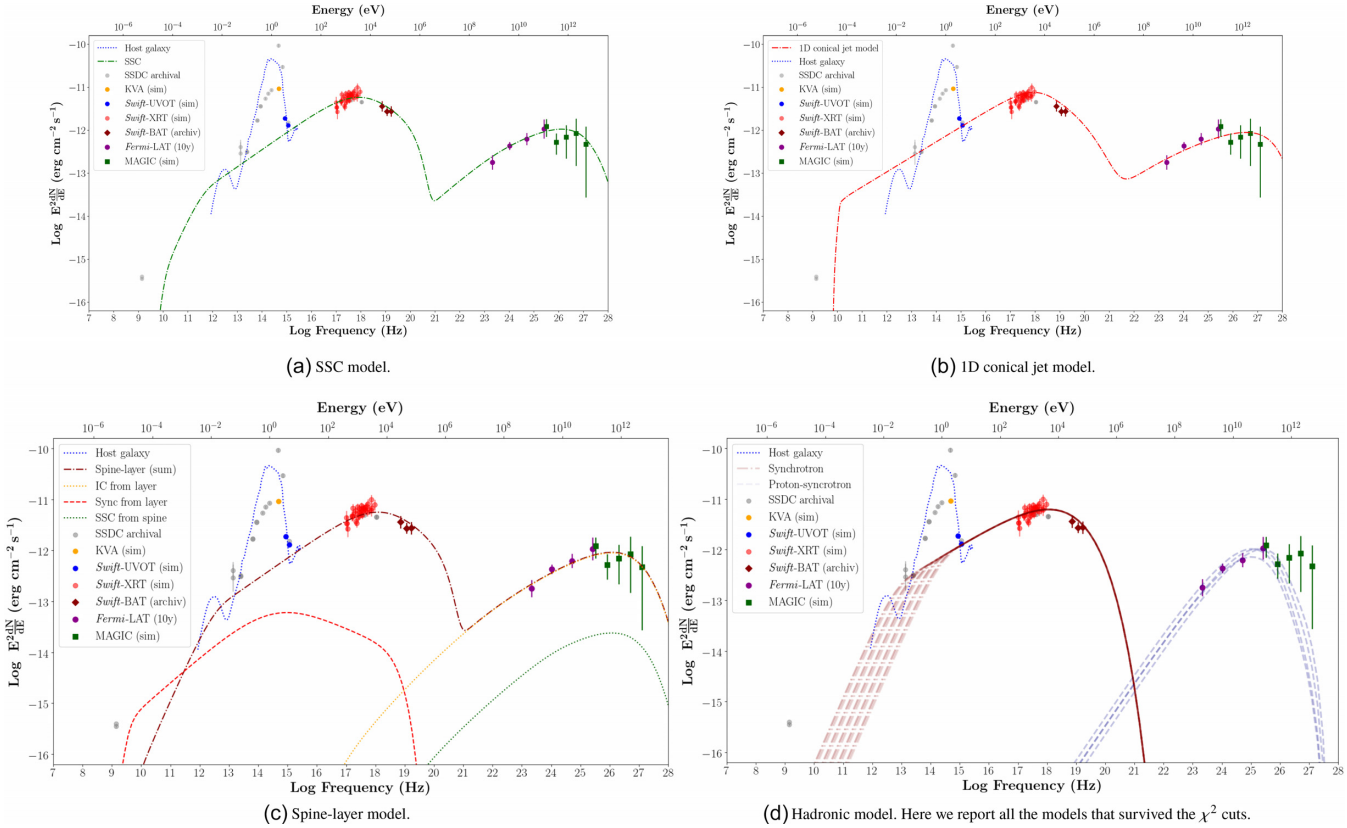

(a) SSC model.

(b) 1D conical jet model.

(c) Spine-layer model.

(d) Hadronic model. Here we report all the models that survived the χ^2 cuts.

Figure 6. MWL intrinsic SED of 2WHSP J073326.7+515354. The data have been EBL deabsorbed using the model by Dominguez et al. (2011). In grey, we report the selected archival SSDC data (*First* data on MJD 49078 in White et al. 1997, *WISE* data between MJD 55287-55479), in orange the KVA data, in light red the *Swift*-XRT data, in dark red the *Swift*-BAT data, in purple the *Fermi*-LAT data, and in dark green the MAGIC data. The arrows represent upper limits.

Table A2, due to the weak detection, the measured flux is compatible with a constant flux during the first 10 yr of operation of *Fermi*-LAT. We checked the possible enhanced flux of the source of interest in the period around January 2014, when there was an optical-UV flux registered by *Swift*-UVOT few times higher with respect to the average flux measured during the MAGIC observation window. An analysis of the *Fermi*-LAT data over the period from 2012 August 3 to 2014 August 3 (MJD 56142.7-56872.7, as reported in Table A2), which includes 2014 January, reports no photons detected with probability >50 per cent of belonging to the source of interest. This result is also compatible with the variability index of 39 reported in the *Fermi*-LAT 3FGL catalogue (Acero et al. 2015), statistically consistent with a steady source (variability threshold 72.44 as reported in the 3FGL catalogue). Moreover, the long-term SED measured by *Fermi*-LAT connects smoothly with the VHE gamma-ray SED observed by MAGIC as shown in Fig. 6. Thus, while short-term variability cannot be excluded due to the low photon statistics and the fact that the long integration of the signal might smooth out some modest flux variations, the stability of the light curve on the long-term supports a steady flux condition of the source within the sensitivity of the instrument.

For the VHE band, as shown in Fig. 4, the source is detected above 2σ C.L. only during four nightly observations (blue points and arrows). The rest of the observations yield upper limits. Due to the lack of strong variability detected from the nightly observations (constant fit with χ^2/DOF of 16/21) and the low photon statistics, the monthly light curve is also evaluated (black points). Also with larger time bins, the light curve does not show any hint of variability, and the average flux results in $(3.4 \pm 0.4) \times 10^{-12}$ ph cm^{-2} s^{-1} with χ^2/DOF of 1.2/4.

In summary, when considering only the MWL data simultaneous to the MAGIC observations, no significant variability is identified. Therefore, during the MAGIC observation campaign the source remained in a stable state. Only some moderate variability was measured by *Swift*-UVOT/XRT when comparing with historical observations.

4 MULTIWAVELENGTH SED

We present in Fig. 6 the SED with the full data sample we assembled for 2WHSP J073326.7+515354. In grey, we show the selected archival SSDC data (see caption for details). Then we report in orange the KVA data, in blue the *Swift*-UVOT data, in light red the *Swift*-XRT data, in dark red the *Swift*-BAT data, in purple the *Fermi*-LAT data, and in dark green the MAGIC data. In order to account for the modest variability found with the *Swift* data, we will consider only its data strictly simultaneous to MAGIC observations (MJD 58144, 58164, 58190, and 58227).

Since the synchrotron peak position $\nu_{\rm peak}^{\rm sync}$ is the basis of the definition of EHBL, this value plays an important role in classifying new sources of this class. In order to measure $\nu_{\rm peak}^{\rm sync}$, we performed a log-parabolic fit of the synchrotron peak of 2WHSP J073326.7+515354 as illustrated in Fig. B1(a). The fit performed only on the *Swift*-XRT X-ray data simultaneous to MAGIC observations, being compatible with a power-law model, does not allow us to constrain the synchrotron peak location. For this reason, the non-simultaneous

Downloaded from https://academic.oup.com/mnras/article/490/2/2284/5579033 by guest on 10 June 2024

Table 2. Resulting values of the parameters used by the three leptonic models in the paper. We report the bulk Lorentz factor Γ, the magnetic field B, and the electron luminosity L_e. The electron distribution is assumed to have an index of p_1 between $\gamma_{\rm min}$ and $\gamma_{\rm br}$, and an index of p_2 up to the maximum $\gamma_{\rm max}$. Then, we report the Compton dominance parameter CD (the ratio of νL_ν at $\varepsilon_{\rm syn,pk}$ to that at $\varepsilon_{\rm IC,pk}$), and the energy density ratio of the magnetic field to that of the non-thermal electron distribution (U_B/U_e) at the radius where the electron injection terminates.

Model	Component	Γ	K	B G	R (R_0/Γ in 1D SSC model) cm	$L_{\rm e}$ erg s^{-1}	$\gamma_{\rm min}$	$\gamma_{\rm br}$	$\gamma_{\rm max}$	p_1	p_2	CD	U_B/U_e
One-zone SSC		30	7.7×10^3	0.01	1×10^{16}	6.2×10^{43}	500	1×10^6	1×10^7	2.2	4.0	0.12	5×10^{-4}
1D SSC		30		0.005	2.1×10^{16}	1.2×10^{45}	20	2×10^6	2×10^7	2.3	3.5	0.12	7×10^{-5}
Spine-layer	spine	30	7.5×10^1	0.02	3×10^{16}	1.2×10^{45}	1000	9×10^5	8×10^6	2.2	4.1	0.14	0.26
	layer	5	1×10^1	0.1	3.5×10^{16}		1	1×10^4	3×10^6	2	3.5		

Swift-BAT 105-month archival data were used to provide a first estimation of the synchrotron peak. The resulting new estimation leads to $\nu^{\rm sync}_{\rm peak} \simeq 10^{17.8\pm0.3}$ Hz (χ^2/DOF of 19/39). This value is compatible with the estimation reported in the 2WHSP catalogue (Chang et al. 2017) of $\nu^{\rm sync}_{\rm peak,2WHSP} = 10^{17.9}$ Hz and confirms the classification of 2WHSP J073326.7+515354 as an EHBL.

Due to the high-frequency location of the synchrotron peak, the SED exhibits the optical radiation of the host galaxy. The combination of the simultaneous KVA and *Swift*-UVOT data allows us to build a good template for the host galaxy radiation in the optical range of the SED.

Due to the set of MAGIC and *Fermi*-LAT SED points, we are now able to study the IC peak $\nu^{\rm IC}_{\rm peak}$, reported in Fig. B1(b). In the HE gamma-ray band, the *Fermi*-LAT points present a hard spectral index of $\Gamma_{\rm HE} = 1.67 \pm 0.11$. This means that they constitute the rising part of the second SED hump that finally peaks in the TeV gamma-ray band. For this reason, given the hard gamma-ray spectrum, we fitted the (EBL-deabsorbed) second hump with a power-law model, reporting a (χ^2/DOF of 5.2/7) and a slope of 2.13 ± 0.04. Alternatively, the EBL-deabsorbed spectrum can be fitted also with a power-law model with exponential cut-off (χ^2/DOF of 4/8). This allows for an estimation of the cut-off $\nu^{\rm IC}_{\rm cutoff} 10^{27.2\pm0.2}$ Hz, and thus that the second SED hump peaks at $\nu^{\rm IC}_{\rm peak} = 10^{26.4\pm0.6}$ Hz.

The Compton dominance (CD) parameter for the different models, reported in Table 2, is defined as the ratio between the second hump peak luminosity and the synchrotron peak luminosity νL_ν. Considering our estimation of the two SED peaks, this parameter results in $CD \sim 0.12$. This result is compatible with the phenomenological CD trend observed for the gamma-ray blazar sample detected by *Fermi*-LAT reported in Finke (2013): the higher the frequency of the synchrotron peak the lower the CD value. The low value for the CD parameter agrees with the conventional interpretation of poor environments without strong low-energy photon fields around the EHBL relativistic jets preventing the high-energy emission via EC scattering (contrary to the rich external fields in FSRQs for instance).

5 MODELLING

Four different emission models have been tested on the experimental data for the emission of the blazar jet. First, we start with the application of two different one-zone leptonic models. Testing such models, we face the need for applying extremely low magnetization within the emission region. Therefore, we use two different approaches to try to overcome this problem: a two-zone leptonic model and a hadronic model.

In addition, the template for a typical host galaxy contribution is applied to the broad-band SED following Silva et al. (1998), adapted to the redshift of 2WHSP J073326.7+515354 ($z = 0.065$). It is worth to note that this model represents only a reference model for the host galaxy emission, and is not fitted to the data. Differences between the model and some archival data might be due to different apertures adopted by the different instruments, or specific observing conditions, but no detailed information about this is available in the data base. Any conclusion based on the comparison between the model and the data would require much more careful analysis beyond our scope.

Given that no significant variability is observed in the source (see Section 3), we fix the emitting region size to $R = 10^{16}$ cm (a typical value for HBLs).

Finally, considering that electrons and positrons cannot be distinguished from a radiative perspective, we will refer to both populations as electrons.

5.1 One-zone leptonic models

5.1.1 Synchrotron self-Compton model

The synchrotron self-Compton model is the standard one-zone leptonic model historically used to model the MWL emission of BL Lac type objects (e.g. Maraschi et al. 1992; Tavecchio et al. 1998). In this scenario, the emission is produced by relativistic electrons contained in a spherical region of radius $R = 10^{16}$ cm with a tangled and uniform magnetic field B. This region is moving with a bulk Lorentz factor Γ along the axis of a relativistic jet, which forms an angle θ with respect to the observer line of sight. The special relativistic effects are accounted for by the relativistic Doppler factor $\delta = [\Gamma(1 - \beta\cos\theta)]^{-1}$. The model assumes the presence of a population of relativistic electrons of density N distributed with a broken power-law spectrum as a function of the Lorentz factor of the electrons:

$$N(\gamma) = K\,\gamma^{-p_1}\left(1 + \frac{\gamma}{\gamma_b}\right)^{p_1-p_2},$$

where K is the normalization factor, and p_1 and p_2 are the spectral indices, respectively, before and after the spectral break, at which the Lorentz factor of the electrons is $\gamma_{\rm b}$.

Electrons produce synchrotron radiation that is in turn Compton-scattered generating the high-energy SSC continuum. As detailed in Tavecchio et al. (1998), this simple model is fully constrained if a good sampling of the SED (especially around the peaks) and an estimate of the variability time-scale are available. The good data set collected for 2WHSP J073326.7+515354 is therefore quite suitable for the application of this model in Fig. 6(a) and provides strong constraints on the physical parameters of the jet, reported in Table 2.

By applying the SSC model to the data, we can provide an estimation of the synchrotron peak located at $\nu^{\rm sync}_{\rm peak} = 10^{18}$ Hz ($\simeq 4.0$ keV) and an IC peak located at $\nu^{\rm IC}_{\rm peak} = 10^{26.4}$ Hz ($\simeq 1.2$ TeV). These values are in agreement with the observational fits we reported in Section 4.

Downloaded from https://academic.oup.com/mnras/article/490/2/2284/5579033 by guest on 10 June 2024

5.1.2 1D conical jet model

The MWL SED has been modelled also adopting the numerical code by Asano et al. () (see also Asano & Hayashida 2015, 2018), reporting the results in Fig. 6(b). This model calculates the emission from the non-thermal electrons in a conical jet. The evolution of the electron and the photon energy distributions are followed along the motion of the jet. This framework is similar to the BLAZAR code by Moderski, Sikora & Błażejowski (2003), which has been frequently adopted to reproduce blazar spectra (see e.g. Kataoka et al. 2008; Hayashida et al. 2012).

The conical expansion of the jet naturally leads to adiabatic cooling of the electrons. This effect resembles the electron escape in one-zone steady models, which can thus be neglected in this 1D code. The model assumes a continuous injection of non-thermal electrons from the initial radius $R = R_0$ during the dynamical time-scale $R_0/c\Gamma$ in the plasma rest frame. In this time-scale, the injection rate into a given volume V – which is expanding as $V \propto R^2$ – is assumed to be constant. The magnetic field B in the plasma frame evolves as $B = B_0\,(R_0/R)$. We take into account the synchrotron and IC scattering with the Klein–Nishina effect, the γ–γ absorption, the secondary pair injection, the synchrotron self-absorption, and the adiabatic cooling.

The electron energy distribution at injection is assumed as a broken power law with exponential cut-off, where the parameters are low-energy index p_1, high-energy index p_2, and the break energy (Lorentz factor) $\gamma_{\rm br}$, and the cut-off energy $\gamma_{\rm max}$. The minimum Lorentz factor $\gamma_{\rm min}$ is fixed as 20. The electron energy distribution and the photon emission are computed even after electron injection ends, until R reaches $R = 10\,R_0$.

In this paper, considering an on-axis observer (viewing angle θ_v is zero), the jet opening angle is assumed to be $1/\Gamma$, where Γ is the bulk Lorentz factor of the jet. The photon flux is obtained by integrating the emission over the entire jet, taking into account the Doppler boosting by the conically outflowing emission region.

For the steady emission scenario, this model includes eight parameters: the initial radius R_0, the bulk Lorentz factor Γ, the initial magnetic field B_0, the electron Luminosity $L_{\rm e}$, p_1, p_2, $\gamma_{\rm br}$, and $\gamma_{\rm max}$. The results are summarized in Table 2. The model provides a particularly low magnetic field B, and this puts the object far from the equipartition limit by more than five orders of magnitude.

The modelling provides also an estimated synchrotron peak frequency $\nu^{\rm sync}_{\rm peak} = 10^{18}$ Hz ($\simeq 4.0$ keV) and an IC peak frequency $\nu^{\rm IC}_{\rm peak} = 10^{26.5}$ Hz ($\simeq 1.25$ TeV). These values are well in agreement with the observational fits we reported in Section 4.

5.2 The energy equipartition issue

In Table 2, we summarize the resulting parameters for the first two one-zone leptonic models we used. An inspection of the table shows that the parameters are quite similar in both the SSC model and the 1D conical jet model. Both the models present a low magnetic field B of the order of 10^{-2} G. The low magnetic field – together with a relatively large Doppler factor – is generally required by the SSC modelling in order to account for the large separation between the two SED peaks. Since the total electron energy for $p_1 > 2$ is dominated by low-energy electrons, a harder electron spectrum ($p_1 < 2$) well below the energy responsible for the synchrotron peak would make it close to equipartition. A stochastic acceleration model (e.g. Asano et al. 2014b) can generate such a hard spectrum. Dermer et al. (2015) succeeded in reproducing a relation between the spectral index and the peak Compton frequency in blazars with an equipartition model adopting log-parabola electron energy distribution motivated by the stochastic acceleration model. Even with their model, however, the broad-band spectrum of Mrk 501 requires a low magnetization. It may be difficult to make it close to the equipartition for EHBLs even with stochastic acceleration models within one–one or 1D SSC picture (see Asano & Hayashida 2015).

Another common feature of the modelling results is the high value of the minimum energy of the electrons $\gamma_{\rm min}$ (Katarzynski et al. 2006). The extreme values obtained by our models for these parameters might be in tension with those commonly adopted to describe standard HBL via SSC emission. Their values are instead in agreement with the ones commonly required in the modelling of the extreme counterpart of this class of sources, the EHBL objects (Tavecchio et al. 2010, but see also Cerruti et al. 2015 for a comparison of some results on the modelling of other known EHBLs).

In the one-zone leptonic framework, both the standard stationary one-zone model and the 1D conical jet model imply an extremely low magnetic field B of the emitting region that results in a low ratio of the energy densities $U_B/U_{\rm e}$, being far from the equipartition limit. Such conditions are particularly interesting considering that they are not related to flaring episodes of the source, but to their relatively quiescent observed emission. This means that, in the case of leptonic scenarios, a mechanism is expected to continuously keep the emission out of equipartition.

In order to increase the $U_B/U_{\rm e}$ ratio, a solution is to decrease the number of radiating electrons and increase the minimum Lorentz factor $\gamma_{\rm min}$. Another way would be to modify the size of the emitting region. A larger size of the emitting region R and smaller Doppler factors δ may be an alternative solution, but these *ad hoc* values would not help enough in bringing the conditions much closer to equipartition, accounting only for few times closer, and not orders of magnitude (e.g. Costamante et al. 2018).

Alternative solutions that require less extreme parameters are proposed in the following sections: a spine-layer structured jet and a hadronic model.

5.3 Two-zone model

5.3.1 Spine-layer model

As shown above, the one-zone models applied to the data of 2WHSP J073326.7+515354 suggest that the emission region is quite far from equipartition, with the electron energy density dominating over that of the magnetic field by more than three orders of magnitude. As discussed by Tavecchio & Ghisellini (2016), this result is commonly found for one-zone models of high-energy-emitting BL Lacs (see also Inoue & Tanaka 2016). The same authors show that a possible solution allowing equipartition conditions for the emitting region is the spine-layer model introduced by Ghisellini, Tavecchio & Chiaberge (2005). In this framework, the relativistic jet is supposed to be structured, as suggested by several theoretical and observational hints (e.g. Tavecchio & Ghisellini 2015 for details). Besides the emission from blazars, the scenario can satisfactorily reproduce the emission of radiogalaxies (Tavecchio & Ghisellini 2008), and can potentially account for the neutrino production in BL Lac objects (Ansoldi et al. 2018).

Specifically, the jet is supposed to consist of two components: a central fast spine and a slower layer around it. The former moves with Lorentz factor $\Gamma_{\rm spine} = 10$–20 in the inner part of the cylindrical jet, while the external layer has $\Gamma_{\rm layer} = 2$–5 (Chhotray et al. 2017).

Downloaded from https://academic.oup.com/mnras/article/490/2/2284/5579033 by guest on 10 June 2024

The layer acts as a source of soft (synchrotron) photons that, due to boosting due to the relative motion of the two jet components, can dominate the radiation energy density in the frame of the spine. In these conditions, the IC emission from the spine is dominated by the scattering of the layer radiation field, while the SSC component is expected to provide a minor contribution. Due to the larger Lorentz factor, at small angles (such as those characterizing blazars) the spine emission prevails over that of the layer.

In Fig. 6(c), we report the model obtained within the spine-layer framework. The IC emission of the spine is largely dominated by the scattering of the layer radiation field. The parameters for the spine (analogous to those describing the one-zone model above) are reported in Table 2.

The introduction of a more complex structure of the jet allows a more relaxed fit of the physical parameters. The spine-layer scheme offers an increased energy density of the radiation field (supposed to be dominated by the radiation provided by the layer), and this allows us to lower the electron density needed to produce a given IC luminosity. In turn, in order to account for the reduced number of electrons, the model slightly increases the magnetic field B to keep the same synchrotron luminosity. This fact increases the previous U_B/U_e ratio and brings it closer the equipartition limit, reconciling it with the theoretical expectations. Also adopting lower values of $\gamma_{\rm min}$ confirms our results concerning the energy densities close to equipartition in this model: for example, $\gamma_{\rm min} = 10$ implies $U_B/U_e = 0.1$, which still represents an acceptable value.

The structured jet model provides more appropriate physical conditions closer to equipartition, and leads to an interesting comparison with its application to the sample of hard-TeV blazars reported in Costamante et al. (2018). In fact, the spine-layer model can provide larger magnetic field that generates a more efficient cooling of the TeV electrons, providing a softer spectrum at TeV energies that does not agree with the hard spectrum up to several TeV of the hard-TeV blazars seen in Costamante et al. (2018).

However, such a softer spectrum at TeV energies is observed in more 'standard' HBL-like EHBLs, like for example 2WHSP J073326.7+515354. This source, according to the results in gamma rays previously found, is an EHBL object that presents an IC peak well detectable at few TeV. This implies that the spine-layer model is still able to fit the SED (especially the IC peak). Thus, the case of 2WHSP J073326.7+515354 might be a limit case in the EHBL population with a high synchrotron peak but not extremely hard TeV gamma-ray spectrum. This result confirms the great difference that might be hidden in the EHBL population due to different spectral properties in the TeV gamma-ray band. Further observations at TeV energies will be able to increase the statistics and characterize new objects of this population.

Applying this model to the data, it provides the synchrotron peak located at $\nu^{\rm sync}_{\rm peak} = 10^{18}$ Hz ($\simeq 4.1$ keV) and an IC peak located at $\nu^{\rm IC}_{\rm peak} = 10^{26.5}$ Hz ($\simeq 1.25$ TeV). These values are in good agreement with the observational fits we reported in Section 4.

5.4 Hadronic model

Another solution in order to interpret the SED of 2WHSP J073326.7+515354 without using extreme physical parameters can be found considering a hadronic origin for the gamma-ray component. Blazar hadronic models, in which the gamma-ray component is ascribed to emission by protons in the jet, or by secondary leptons produced in p–gamma interactions, have been widely studied (e.g. Mannheim 1993; Aharonian 2000; Mucke & Protheroe 2001; Boettcher et al. 2013) as an alternative to leptonic models. One of the major drawbacks of this scenario is that it often requires a high proton power, well above the Eddington luminosity of the black hole powering the blazar. For the particular case of EHBLs on the other hand, due to their relatively low luminosity compared to other blazar subclasses, a successful hadronic modelling can be achieved with an acceptable energy budget (see Cerruti et al. 2015). In addition, the absence of fast flares from EHBLs (in contrast with the γ-ray variability seen in more common HBLs) is also consistent with the cooling time-scales of protons in the jet. With this scenario in mind, we test a simple proton-synchrotron model for 2WHSP J073326.7+515354, using the numerical code described in Cerruti et al. (2015). We make the following assumptions to reduce the number of free parameters to study:

(i) electrons and protons share the same acceleration process, and thus the index α of the injected energy distribution is identical;
(ii) the maximum proton Lorentz factor $\gamma_{\rm p,max}$ is constrained by the equality of cooling and acceleration time-scales; for the parameters used in the model, the fastest cooling time-scale for protons is the adiabatic one;
(iii) the electron energy distribution at equilibrium is calculated assuming that electrons are cooled primarily by synchrotron radiation;
(iv) the emitting region size R is limited by the variability time-scale, which is considered to be two days
(v) the Doppler factor δ of the emitting region is fixed to 30.

Under these assumptions, we produce 350 hadronic models scanning the following parameter space: the radius of the emitting region $R \in [10^{14}$–$1.46 \times 10^{17}]$ cm, the proton peak synchrotron frequency $\nu_{\rm p,syn} \in [4 \times 10^{24}$–$4 \times 10^{26}]$ Hz, and the proton normalization $K_{\rm p} \in [K^\star/3, 3K^\star]$, where $K^\star$ corresponds to the proton density such that the peak of the proton-synchrotron component is at the level of the MAGIC data. A χ^2 test is used to select the solutions which correspond to a 1σ C.L., obtaining the best χ^2/DOF of 46/42. The proton-synchrotron models which describe the SED are shown in Fig. 6(d) and the corresponding model parameters are reported in Table 3.

Hadronic solutions are thus a viable alternative to leptonic ones, and can be achieved with acceptable values for the Doppler factor (equal to 30) and the jet luminosity (which can be as low as 2×10^{45} erg s^{-1}, which is about $0.01 \times L_{\rm Edd}$ for a typical supermassive black hole mass of 10^9 solar masses). The emitting region in this case is extremely out of equipartition, being dominated by the magnetic energy density with $U_B/U_{\rm p} \simeq 0.9$–120×10^3. The well-known degeneracy in the synchrotron radiation spectrum implies that the parameters of the emitting region cannot be constrained, and indeed all studied values of the size of the emitting region from $R_{\rm min} = 10^{14}$ cm to $R_{\rm max} = 1.46 \times 10^{17}$ cm can provide a good solution. The same is true for the values of the magnetic field, which can take any value between 1.2 and 46.8 G. The only parameter which takes unusual values is the index of the injected particle population, $\alpha = 1.3$: such a hard injection index is not consistent with standard shock acceleration, although it can be achieved if particles are accelerated via magnetic reconnection (Sironi & Spitkovsky 2014). On the other hand, it is important to underline that this value does not come from the SED fitting, but is a direct consequence of the two assumptions on co-acceleration of electrons and protons, and that only synchrotron and adiabatic cooling terms shape the stationary particle distribution. Removing one of these assumptions (or both)

Downloaded from https://academic.oup.com/mnras/article/490/2/2284/5579033 by guest on 10 June 2024

Table 3. Parameters used for the hadronic model. The luminosity of the emitting region has been calculated as $L = 2\pi R^2 c \Gamma^2_{\rm bulk}(u_B + u_{\rm e} + u_{\rm p})$, where $\Gamma_{\rm bulk} = \delta/2$, and u_B, $u_{\rm e}$, and $u_{\rm p}$, the energy densities of the magnetic field, the electrons, and the protons, respectively. The quantities flagged with a star (*) are derived quantities, and not model parameters.

	Proton synchrotron
δ	*30*
R [10^{16} cm]	0.1–14.6
$^\star\tau_{\rm obs}$ [h]	0.3–48.0
B [G]	1.2–46.8
$^\star u_B$ [erg cm^{-3}]	0.06–87
$\gamma_{\rm e,min}$	200
$\gamma_{\rm e,break}$	$= \gamma_{e,\rm min}$
$\gamma_{\rm e,max}$ [10^4]	2.5–15.6
$\alpha_{\rm e,1} = \alpha_{\rm p,1}$	1.3
$\alpha_{\rm e,2} = \alpha_{\rm p,2}$	2.3
$K_{\rm e}$ [10^{-3} cm^{-3}]	0.015–311
$^\star u_{\rm e}$ [10^{-7} erg cm^{-3}]	0.013–249
$\gamma_{\rm p,min}$	1
$\gamma_{\rm p,break}$[10^9]	$= \gamma_{p,\rm max}$
$\gamma_{\rm p,max}$[10^9]	2.2–15.7
η [10^{-5}]	0.26–2.6
$^\star u_{\rm p}$ [10^{-4} erg cm^{-3}]	0.009–10.7
$^\star U_B/U_{\rm p}$ [10^3]	0.9–120
$^\star L$ [10^{46} erg s^{-1}]	0.2–10.3

can lead to softer particle injection indices still in agreement with the observations.

The hadronic model provides an estimated synchrotron peak located at $\nu^{\rm sync}_{\rm peak} = 10^{18}$ Hz ($\simeq 4.1$ keV) and a gamma-ray peak located at $\nu_{\rm peak} = (2\text{–}4) \times 10^{25}$ Hz ($\simeq 0.25$ TeV). The latter range of values represents the result for the best-fitting solutions whose χ^2 is dominated by the *Fermi*-LAT data.

6 CONCLUSIONS

In this work, we provide the results of the TeV gamma-ray discovery of the EHBL 2WHSP J073326.7+515354. This source has been observed during 2018 with the MAGIC telescopes, which reported a firm detection after about 23 h of observations. Simultaneous data have been collected also in the optical, UV, soft X-ray, and HE gamma-ray bands. This allowed us to build a well-sampled broad-band SED of the source. Due to the new data for this source, we were also able to perform a new estimation of the synchrotron peak and IC peak positions. This leads us to confirm the classification of this source as an EHBL object but showing a softer spectrum at gamma rays compared to the 'hard-TeV' EHBLs like for example 1ES 0229+200.

The broad-band SED has been fitted with four different models: three leptonic and one hadronic. The results of leptonic SSC models, whether considering electron acceleration in a spherical plasmoid or in the whole conical expansion of the jet, substantially agree on the extreme spectral parameters needed to fit the SED of this source. The high Doppler factor δ, the low magnetic field B of the emitting region, and the minimum Lorentz factor $\gamma_{\rm min}$ are common resulting parameters. However, for the one-zone leptonic framework an extremely low magnetization is required, in both models being very far from equipartition. In order to overcome this problem, two different approaches are used: a two-zone leptonic model (spine-layer), and a hadronic scenario. While the one-zone leptonic models result in a ratio between the energy density of the particles and the magnetic field ($U_{\rm e}/U_B$) of several orders of magnitude, the spine-layer model results in a value close to the theoretical expectations. Another interesting point is that equipartition is not reachable with the spine-layer model in other EHBLs like the 'hard-TeV' blazars (e.g. 1ES 0229+200), and this implies that this object might represent an exception or a transitional case in the EHBL class where the spectral properties are sufficiently extreme but the equipartition regime still holds with respect to hard-TeV blazars (compare with Costamante et al. 2018).

The relatively low luminosity of EHBLs and their modest variability make the application of hadronic modelling successful with reasonable physical parameters. Therefore, in addition to the leptonic models, we presented another model by including a hadronic contribution to the emission mechanism. While the hadronic scenario is able to produce a plausible fit to the MWL SED, the opposite problem for equipartition with respect to one-zone leptonic models is found. The parameter space able to fit the SED results in a ratio $U_B/U_{\rm e}$ far from equipartition, with the jet highly magnetized in this case. For all the models we tested, we ignored the cascade emission by pairs produced in the interaction of TeV photons with the EBL. Emission from these pairs could emerge in the MeV–GeV part of the spectrum if pairs are not isotropized by the IGMF, or if they do not loose energy via other mechanisms. Such an emission, although predicted theoretically, has never been observed so far in any gamma-ray blazar, indicating that, if it exists, it is likely sub-dominant with respect to the emission from the source itself. Finally, considering that the simple one-zone SSC model already provides a good description of the SED, more complex models (including hadronic component, e.g. a photomeson model similar to that discussed in MAGIC Collaboration 2018) could only provide second-order effects.

In conclusion, while the four SED modelling scenarios can provide compatible models for the MWL SED of 2WHSP J073326.7+515354, extreme physical parameters would be required for three of them. The model that better matches with the theoretical predictions is the spine-layer scenario, which provides a reasonable framework to explain the broad-band SED.

The case of 2WHSP J073326.7+515354 is an important example of the key role that the TeV gamma-ray band plays in the characterization of EHBLs. New observations of this class of sources by Cherenkov telescopes will allow to increase the number of objects in this population. The forthcoming Cherenkov Telescope Array (CTA) observatory, with its improved sensitivity in this energy band, will be critical in discovering new TeV EHBLs and will help in disclosing the physical phenomena behind their extreme spectral emission.

ACKNOWLEDGEMENTS

We would like to thank the Instituto de Astrofísica de Canarias for the excellent working conditions at the Observatorio del Roque de los Muchachos in La Palma. The financial support of the German BMBF and MPG, the Italian INFN and INAF, the Swiss National Fund SNF, the ERDF under the Spanish MINECO (FPA2017-87859-P, FPA2017-85668-P, FPA2017-82729-C6-2-R, FPA2017-82729-C6-6-R, FPA2017-82729-C6-5-R, AYA2015-71042-P, AYA2016-76012-C3-1-P, ESP2017-87055-C2-2-P, FPA2017-90566-REDC), the Indian Department of Atomic

Downloaded from https://academic.oup.com/mnras/article/490/2/2284/5579033 by guest on 10 June 2024

Energy, the Japanese JSPS and MEXT, the Bulgarian Ministry of Education and Science, National RI Roadmap Project DO1-153/28.08.2018 and the Academy of Finland grant nr. 320045 is gratefully acknowledged. This work was also supported by the Spanish Centro de Excelencia 'Severo Ochoa' SEV-2016-0588 and SEV-2015-0548, and Unidad de Excelencia 'María de Maeztu' MDM-2014-0369, by the Croatian Science Foundation (HrZZ) Project IP-2016-06-9782 and the University of Rijeka Project 13.12.1.3.02, by the DFG Collaborative Research Centers SFB823/C4 and SFB876/C3, the Polish National Research Centre grant UMO-2016/22/M/ST9/00382 and by the Brazilian MCTIC, CNPq and FAPERJ.

The *Fermi* LAT Collaboration acknowledges generous ongoing support from a number of agencies and institutes that have supported both the development and the operation of the LAT as well as scientific data analysis. These include the National Aeronautics and Space Administration and the Department of Energy in the United States, the Commissariat à l'Energie Atomique and the Centre National de la Recherche Scientifique / Institut National de Physique Nucléaire et de Physique des Particules in France, the Agenzia Spaziale Italiana and the Istituto Nazionale di Fisica Nucleare in Italy, the Ministry of Education, Culture, Sports, Science and Technology (MEXT), High Energy Accelerator Research Organization (KEK) and Japan Aerospace Exploration Agency (JAXA) in Japan, and the K. A. Wallenberg Foundation, the Swedish Research Council and the Swedish National Space Board in Sweden.

Additional support for science analysis during the operations phase is gratefully acknowledged from the Istituto Nazionale di Astrofisica in Italy and the Centre National d'Études Spatiales in France. This work performed in part under DOE Contract DE-AC02-76SF00515.

We acknowledge the use of public data from the *Swift* data archive. This publication uses data products from the Wide-field Infrared Survey Explorer, which is a joint project of the University of California, Los Angeles, and the Jet Propulsion Laboratory/California Institute of Technology, funded by the National Aeronautics and Space Administration. We also acknowledge the use of the Space Science Data Base (SSDC).

JBG acknowledges the support of the Viera y Clavijo program funded by ACIISI and ULL. MC has received financial support through the Postdoctoral Junior Leader Fellowship Programme from la Caixa Banking Foundation, grant no. LCF/BQ/LI18/11630012.

REFERENCES

Abdo A. A. et al., 2010, ApJ, 716, 30
Acciari V. A. et al., 2010, ApJ, 715, L49
Acero F. et al., 2015, ApJS, 218, 23
Acero F. et al., 2016, ApJS, 223, 26
Aharonian F. A., 2000, New Astron., 5, 377
Aharonian F. et al., 2007a, A&A, 470, 475
Aharonian F. et al., 2007b, A&A, 473, L25
Aharonian F. et al., 2007c, A&A, 475, L9
Ahnen M. L., et al., 2018, A&A, 620, A181
Ajello M. et al., 2017, ApJS, 232, 18
Albert J. et al., 2007, Astropart. Phys., to Submitted
Aleksić J. et al., 2016a, Astropart. Phys., 72, 61
Aleksić J. et al., 2016b, Astropart. Phys., 72, 76
Aliu E. et al., 2014, ApJ, 782, 13
Ansoldi S. et al., 2018, ApJ, 863, L10
Antón S., Browne I. W. A., 2005, MNRAS, 356, 225
Arsioli B., Barres de Almeida U., Prandini E., Fraga B., Foffano L., 2018, MNRAS, 480, 2165
Asano K., Hayashida M., 2015, ApJ, 808, L18
Asano K., Hayashida M., 2018, ApJ, 861, 31
Asano K., Takahara F., Kusunose M., Toma K., Kakuwa J., 2014b, ApJ, 780, 64
Atwood W. B. et al., 2009, ApJ, 697, 1071
Becerra Gonzalez J., Clavero R., Peralta de Arriba L., Acosta J. A., Garcia Lopez R., 2018, Astron. Telegram, 11621, 1
Boettcher M., 2010, in Savolainen T., Ros E., Porcas R. W., Zensus J. A., eds, Fermi Meets Jansky - AGN at Radio and Gamma-Rays, 41, preprint (arXiv:1006.5048)
Boettcher M., Reimer A., Sweeney K., Prakash A., 2013, ApJ, 768, 54
Breeveld A. A. et al., 2010, MNRAS, 406, 1687
Burrows D. N. et al., 2004, in Flanagan K. A., Siegmund O. H. W., eds, Proc. SPIE Conf. Ser., Vol. 5165. X-Ray and Gamma-Ray Instrumentation for Astronomy XIII. SPIE, Bellingham, p. 201
Cardelli J. A., Clayton G. C., Mathis J. S., 1989, ApJ, 345, 245
Cerruti M., Zech A., Boisson C., Inoue S., 2015, MNRAS, 448, 910
Chang Y. -L., Arsioli B., Giommi P., Padovani P., 2017, A&A, 598, A17
Chhotray A., Nappo F., Ghisellini G., Salafia O. S., Tavecchio F., Lazzati D., 2017, MNRAS, 466, 3544
Costamante L. et al., 2001b, A&A, 371, 512
Costamante L., Bonnoli G., Tavecchio F., Ghisellini G., Tagliaferri G., Khangulyan D., 2018, MNRAS, 477, 4257
Da Vela P., Stamerra A., Neronov A., Prandini E., Konno Y., Sitarek J., 2018, Astropart. Phys., 98, 1
Dermer C. D., Schlickeiser R., 1993, ApJ, 416, 458
Dermer C. D., Yan D., Zhang L., Finke J. D., Lott B., 2015, ApJ, 809, 174
Dominguez A. et al., 2011, MNRAS, 410, 2556
Essey W., Kusenko A., 2010, Astropart. Phys., 33, 81
Evans P. A. et al., 2009, MNRAS, 397, 1177
Fallah Ramazani V., Lindfors E., Nilsson K., 2017, A&A, 608, A68
Finke J. D., 2013, ApJ, 763, 134
Foffano L., Prandini E., Franceschini A., Paiano S., 2019, MNRAS, 486, 1741
Fossati G., Maraschi L., Celotti A., Comastri A., Ghisellini G., 1998, MNRAS, 299, 433
Ghisellini G., 1999, Astropart. Phys., 11, 11
Ghisellini G., Tavecchio F., 2008, MNRAS, 387, 1669
Ghisellini G., Tavecchio F., Chiaberge M., 2005, A&A, 432, 401
Ghisellini G., Righi C., Costamante L., Tavecchio F., 2017, MNRAS, 469, 255
Giommi P., Padovani P., Polenta G., Turriziani S., D'Elia V., Piranomonte S., 2012, MNRAS, 420, 2899
Hauser M. G., Dwek E., 2001, ARA&A, 39, 249
Hayashida M. et al., 2012, ApJ, 754, 114
Inoue Y., Tanaka Y. T., 2016, ApJ, 828, 13
Kalberla P. M. W., Burton W. B., Hartmann D., Arnal E. M., Bajaja E., Morras R., Pöppel W. G. L., 2005, A&A, 440, 775
Kataoka J. et al., 2008, ApJ, 672, 787
Katarzynski K., Ghisellini G., Mastichiadis A., Tavecchio F., Maraschi L., 2006, A&A, 453, 47
Lefa E., Rieger F. M., Aharonian F., 2011, ApJ, 740, 64
Li T.-P., Ma Y.-Q., 1983, ApJ, 272, 317
MAGIC Collaboration, 2018, MNRAS, 480, 879
Mannheim K., 1993, A&A, 269, 67
Maraschi L., Ghisellini G., Celotti A., 1992, ApJ, 397, L5
Martino L., Elvira V., 2017, preprint (arXiv:1704.04629)
Mirzoyan R., 2018, Astron. Telegram, 11548, 1
Mizobuchi S., Aliu E., Mazin D., Teshima M., Wagner R. M., Wittek W., Yoshii H., 2005, in Proceedings, 29th International Cosmic Ray Conference (ICRC 2005). India, p. 323
Moderski R., Sikora M., Błażejowski M., 2003, A&A, 406, 855
Moralejo A. et al., 2009, preprint (arXiv:e-print)

Downloaded from https://academic.oup.com/mnras/article/490/2/2284/5579033 by guest on 10 June 2024

Mucke A., Protheroe R. J., 2001, in 27th International Cosmic Ray Conference (ICRC 2001), August 7-15, 2001. Hamburg, Germany, p. 1153
Murase K., Dermer C. D., Takami H., Migliori G., 2012, ApJ, 749, 63
Nilsson K. et al., 2018, A&A, 620, A185
Oh K. et al., 2018, ApJS, 235, 4
Pian E. et al., 1998, ApJ, 492, L17
Planck Collaboration VI, 2018, preprint (arXiv:1807.06209)
Poole T. S. et al., 2008, MNRAS, 383, 627
Rees M. J., 1967, MNRAS, 135, 345
Saugé L., Henri G., 2004, ApJ, 616, 136
Schlafly E. F., Finkbeiner D. P., 2011, ApJ, 737, 103
Silva L., Granato G. L., Bressan A., Danese L., 1998, ApJ, 509, 103
Sironi L., Spitkovsky A., 2014, ApJ, 783, L21
Tavecchio F., 2014, MNRAS, 438, 3255
Tavecchio F., Ghisellini G., 2008, MNRAS, 385, L98
Tavecchio F., Ghisellini G., 2015, MNRAS, 451, 1502
Tavecchio F., Ghisellini G., 2016, MNRAS, 456, 2374
Tavecchio F., Maraschi L., Ghisellini G., 1998, ApJ, 509, 608
Tavecchio F., Ghisellini G., Ghirlanda G., Costamante L., Franceschini A., 2009, MNRAS, 399, L59
Tavecchio F., Ghisellini G., Ghirlanda G., Foschini L., Maraschi L., 2010, MNRAS, 401, 1570
The Fermi-LAT collaboration, 2019, preprint (arXiv:1902.10045)
Vovk I., Taylor A. M., Semikoz D., Neronov A., 2012, ApJ, 747, L14
White R. L., Becker R. H., Helfand D. J., Gregg M. D., 1997, ApJ, 475, 479

APPENDIX A: OBSERVATION TABLES

In this appendix, the tables including the MWL observation results are included. The nightly fluxes obtained in the VHE band as observed by MAGIC telescopes are given in Table A1. The two-year fluxes obtained in the HE band with the *Fermi*-LAT telescope are reported in Table A2. In Tables A3 and A4 we report the information from all the observations of the source with the *Swift*-XRT and *Swift*-UVOT instruments, respectively. The details from the optical observations from KVA telescope are reported in Table A5.

Table A1. Flux (points and 95 per cent C.L. upper limits) and effective observing time of the source 2WHSP J073326.7+515354 registered by the MAGIC telescopes.

Date MJD	Effective time s	Flux$_{>200\,\mathrm{GeV}}$ 10^{-12} ph cm^{-2} s^{-1}
58141.1	2762	<9.46
58142.1	2584	<12.35
58143.1	2331	<19.45
58144.1	2392	<16.00
58164.1	2350	<8.41
58165.1	2350	<3.09
58167.1	2442	<8.09
58169.0	3355	<12.23
58171.0	7938	2.97 ± 1.86
58185.9	1363	<10.59
58190.0	3126	<13.40
58194.0	5047	3.68 ± 2.51
58194.9	4372	<10.41
58195.9	2350	5.92 ± 3.92
58196.9	2350	<12.20
58198.9	4598	<10.64
58199.9	5550	<7.50
58210.9	3496	<11.93
58211.9	7010	<6.75
58213.9	4682	5.11 ± 2.77
58226.9	2342	<16.05

Table A2. *Fermi*-LAT light curve generated for two-year time bins within the 0.5–300 GeV energy band. In case of non-significant detection (TS < 4), a 95 per cent C.L. flux upper limit was estimated assuming the spectral index reported in the 4FGL catalogue.

MJD$_{start}$	MJD$_{stop}$	Flux 10^{-10} ph cm^{-2} s^{-1}	Γ	TS
54682.7	55412.7	2.6 ± 1.1	1.4 ± 0.2	45.6
55412.7	56142.7	3.2 ± 1.4	1.6 ± 0.2	25.1
56142.7	56872.7	6.8 ± 2.0	1.8 ± 0.2	58.8
56872.7	57602.7	1.9 (U.L.)	1.7	0.4
57602.7	58332.7	1.6 ± 1.1	1.5 ± 0.4	15.9

Table A3. Results of *Swift*-XRT data analysis for the observations of 2WHSP J073326.7+515354. We report for each observation the MJD, the exposure obtained by XRT, and the two integral fluxes between 2–10 and 0.3–10 keV. Every individual spectrum can be well fitted by a power-law function with spectral index Γ_X and good reduced χ^2. In addition to the simultaneous observations with MAGIC, the results from historical observations are also included for comparison purposes.

Date	MJD	Exposure s	$F_{2-10\,\mathrm{keV}}$ 10^{-11} erg cm^{-2} s^{-1}	$F_{0.3-10\,\mathrm{keV}}$ 10^{-11} erg cm^{-2} s^{-1}	Γ_X	χ^2/DOF	Obs. ID
2009-12-30	55195.8	1061	1.36 ± 0.16	2.12 ± 0.17	1.71 ± 0.08	15.59/17	00038675001
2011-02-20	55612.2	9872	0.84 ± 0.03	1.34 ± 0.04	1.76 ± 0.03	117.16/112	00045364001
2011-02-24	55616.4	492	0.57 ± 0.18	1.13 ± 0.19	2.07 ± 0.21	0.38/3	00045364002
2014-01-11	56668.7	1096	1.90 ± 0.16	2.99 ± 0.16	1.73 ± 0.06	20.17/25	00048299002
2014-01-12	56669.7	994	1.91 ± 0.17	2.89 ± 0.19	1.67 ± 0.07	17.44/21	00048299003
2018-01-26	58144.1	1326	1.32 ± 0.11	1.95 ± 0.10	1.62 ± 0.06	27.66/25	00010541001
2018-02-07	58156.0	1364	1.03 ± 0.09	1.72 ± 0.09	1.82 ± 0.06	22.24/26	00010541002
2018-02-15	58164.0	1059	1.62 ± 0.20	2.27 ± 0.19	1.51 ± 0.09	20.33/16	00010541003
2018-02-22	58171.9	1004	1.80 ± 0.19	2.58 ± 0.20	1.55 ± 0.07	19.94/18	00010541004
2018-03-06	58183.9	1441	1.14 ± 0.10	1.79 ± 0.11	1.72 ± 0.07	26.28/25	00010541006
2018-03-12	58190.0	1419	1.40 ± 0.12	2.08 ± 0.13	1.62 ± 0.06	22.83/29	00010541007
2018-04-08	58216.4	1094	1.42 ± 0.12	2.18 ± 0.14	1.68 ± 0.07	29.56/23	00010541009
2018-04-19	58227.9	1136	1.09 ± 0.09	1.84 ± 0.11	1.84 ± 0.07	38.97/24	00010541010

Downloaded from https://academic.oup.com/mnras/article/490/2/2284/5579033 by guest on 10 June 2024

Table A4. Results of *Swift*-UV data analysis for the observations of 2WHSP J073326.7+515354. We report the energy band of the UVOT instrument, the date and MJD of the observation, the integral flux, and the compatibility between each value and the average flux for only 2018 data simultaneous to MAGIC observations. The compatibility has been computed as $\lambda = \frac{|A-B|}{\sqrt{\sigma_A^2+\sigma_B^2}}$, for the given two fluxes with values A and B and their respective uncertainties (σ_A and σ_B), where for example A is a flux value and B is the average flux reported in the text.

Band	Date	MJD	Flux 10^{-12} erg cm^{-2} s^{-1}	Compatibility with average flux
U	2011-02-20	55612	1.79 ± 0.10	0.4
	2011-02-24	55616	1.76 ± 0.11	0.1
	2014-01-11	56668	2.38 ± 0.10	5.8
	2018-01-26	58144	1.74 ± 0.08	0.1
	2018-02-07	58156	1.82 ± 0.09	0.7
	2018-02-15	58164	1.63 ± 0.10	1.1
	2018-04-08	58216	1.88 ± 0.11	1.1
W1	2009-12-30	55195	1.40 ± 0.11	0.6
	2018-02-22	58171	1.26 ± 0.10	0.0
	2018-03-06	58183	1.21 ± 0.11	0.2
	2018-04-19	58227	1.29 ± 0.11	0.1
W2	2011-02-20	55612	1.15 ± 0.10	0.3
	2014-01-12	56669	1.83 ± 0.11	4.6
	2018-03-12	58189	1.18 ± 0.08	

Table A5. Optical *R*-band flux of 2WHSP J073326.7+515354 as measured by the KVA telescope. The data have already been corrected by host galaxy subtraction.

MJD	Flux 10^{-4} Jy
58210.500	4.01 ± 0.38
58211.462	3.87 ± 0.39
58212.467	3.89 ± 0.39
58214.479	3.94 ± 0.41
58215.455	3.61 ± 0.60
58218.508	3.85 ± 0.37
58219.465	3.48 ± 0.40
58222.487	4.10 ± 0.40
58226.473	3.55 ± 0.39
58232.497	3.84 ± 0.41
58233.469	2.98 ± 0.44
58241.482	4.00 ± 0.39
58403.851	4.07 ± 0.38
58423.835	3.98 ± 0.39
58471.822	4.41 ± 0.38
58478.822	4.09 ± 0.38
58481.804	4.00 ± 0.38
58482.743	3.94 ± 0.38
58488.802	3.92 ± 0.37

APPENDIX B: ESTIMATION OF THE BROAD-BAND SED PEAK FREQUENCY

The frequencies at which the peaks of the MWL SED are located are crucial for the classification of the target. For the case of 2WHSP J073326.7+515354, the low-energy peak is characterized by means of the *Swift*-XRT and *Swift*-BAT spectra. The high-energy peak instead is characterized by the gamma-ray observations from *Fermi*-LAT and MAGIC. The SEDs can be found in Fig. B1.

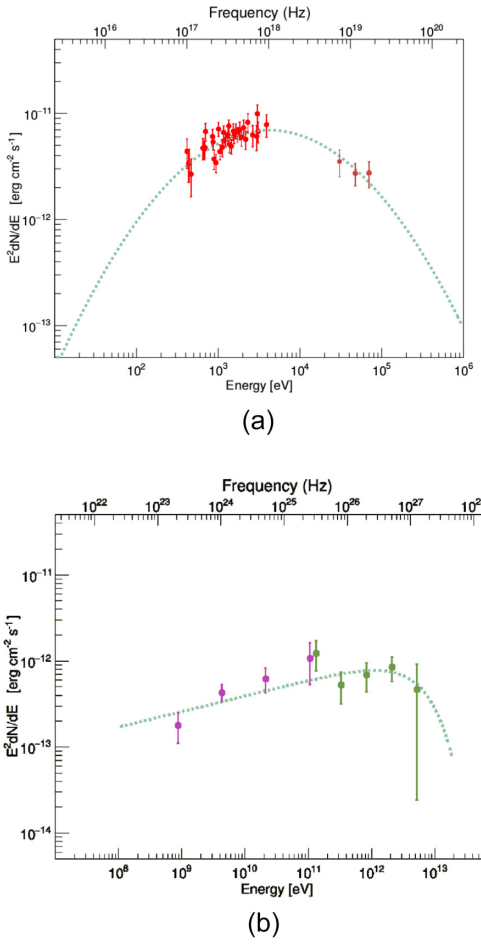

Figure B1. Synchrotron (a) and (b) IC hump of 2WHSP J073326.7+515354. (a) Synchrotron peak of 2WHSP J073326.7+515354. The log-parabolic model fits the simultaneous *Swift*-XRT data (violet dots) and the archival *Swift*-BAT 105-month catalogue (Oh et al. 2018) data (dark red dots). (b) High-energy SED hump of 2WHSP J073326.7+515354. The MAGIC spectral points (blue dots) are EBL corrected using the model from Dominguez et al. (2011). A power law with an exponential cut-off is used to fit the *Fermi*-LAT data (red circles) and the MAGIC data (blue circles).

Downloaded from https://academic.oup.com/mnras/article/490/2/2284/5579033 by guest on 10 June 2024

[1]*Instituto de Astrofísica de Canarias, E-38200 La Laguna, Tenerife, Spain*
[2]*Departamento de Astrofísica, Universidad de La Laguna, E-38206 La Laguna, Tenerife, Spain*
[3]*Università di Udine, and INFN Trieste, I-33100 Udine, Italy*
[4]*ICRR, The University of Tokyo, 277-8582 Chiba, Japan*
[5]*Department of Physics, Kyoto University, 606-8502 Kyoto, Japan*
[6]*Physics department, Tokai University, 259-1292 Kanagawa, Japan*
[7]*RIKEN, 351-0198 Saitama, Japan*
[8]*National Institute for Astrophysics (INAF), I-00136 Rome, Italy*
[9]*ETH Zurich, CH-8093 Zurich, Switzerland*
[10]*Physics department, Technische Universität Dortmund, D-44221 Dortmund, Germany*
[11]*Department of Physics, University of Rijeka, 51000 Rijeka, Croatia*
[12]*Physics department, University of Split - FESB, 21000 Split, Croatia*
[13]*Physics department, University of Zagreb - FER, 10000 Zagreb, Croatia*
[14]*Physics department, University of Osijek, 31000 Osijek, Croatia*
[15]*Physics department, Rudjer Boskovic Institute, 10000 Zagreb, Croatia*
[16]*Saha Institute of Nuclear Physics, HBNI, 1/AF Bidhannagar, Salt Lake, Sector-1, Kolkata 700064, India*
[17]*Centro Brasileiro de Pesquisas Físicas (CBPF), 22290-180 URCA, Rio de Janeiro, RJ, Brasil*
[18]*IPARCOS Institute and EMFTEL Department, Universidad Complutense de Madrid, E-28040 Madrid, Spain*
[19]*Department of Astrophysics, University of Łódź, PL-90236 Łódź, Poland*
[20]*Physics department, Università di Siena, and INFN Pisa, I-53100 Siena, Italy*
[21]*Deutsches Elektronen-Synchrotron (DESY), D-15738 Zeuthen, Germany*
[22]*Physics department, Università di Padova and INFN, I-35131 Padova, Italy*
[23]*Istituto Nazionale Fisica Nucleare (INFN), I-00044 Frascati (Roma), Italy*
[24]*Max-Planck-Institut für Physik, D-80805 München, Germany*
[25]*Institut de Física d'Altes Energies (IFAE), The Barcelona Institute of Science and Technology (BIST), E-08193 Bellaterra (Barcelona), Spain*
[26]*Physics department, Università di Pisa, and INFN Pisa, I-56126 Pisa, Italy*
[27]*ICCUB, Universitat de Barcelona, IEEC-UB, E-08028 Barcelona, Spain*
[28]*ICRANet-Armenia at NAS RA, 0019 Yerevan, Armenia*
[29]*Centro de Investigaciones Energéticas, Medioambientales y Tecnológicas, E-28040 Madrid, Spain*
[30]*Port d'Informació Científica (PIC) E-08193 Bellaterra (Barcelona) Spain*
[31]*Physics department, Universität Würzburg, D-97074 Würzburg, Germany*
[32]*Finnish Centre of Astronomy with ESO (FINCA), University of Turku, FI-20014 Turku, Finland*
[33]*Astronomy Research Unit, University of Oulu, FI-90014 Oulu, Finland*
[34]*Departament de Física, and CERES-IEEC, Universitat Autònoma de Barcelona, E-08193 Bellaterra, Spain*
[35]*Dipartimento di Fisica, Università di Trieste, I-34127 Trieste, Italy*
[36]*Institute for Nuclear Research and Nuclear Energy, Bulgarian Academy of Sciences, BG-1784 Sofia, Bulgaria*
[37]*INAF-Trieste and Department of Physics and Astronomy, University of Bologna, Italy*
[38]*INAF Istituto di Radioastronomia, via Gobetti 101, 40129 Bologna, Italy*

This paper has been typeset from a TEX/LATEX file prepared by the author.

Downloaded from https://academic.oup.com/mnras/article/490/2/2284/5579033 by guest on 10 June 2024